

Received August 3, 2017, accepted August 27, 2017, date of publication October 2, 2017, date of current version October 25, 2017.

Digital Object Identifier 10.1109/ACCESS.2017.2755984

# Role of Self-Heating and Polarization in AlGa<sub>N</sub>/Ga<sub>N</sub>-Based Heterostructures

KHALED AHMEDA<sup>1</sup>, BRENDAN UBOCHI<sup>1</sup>, BRAHIM BENBAKHTI<sup>2</sup>, STEVEN J. DUFFY<sup>2</sup>, ALI SOLTANI<sup>3,4</sup>, WEI DONG ZHANG<sup>2</sup>, AND KAROL KALNA<sup>1</sup>

<sup>1</sup>Nanoelectronic Devices Computational Group, College of Electronic and Electrical Engineering, Swansea University, Swansea SA2 8PP, U.K.

<sup>2</sup>Department of Electronics and Electrical Engineering, Liverpool John Moores University, Liverpool L3 3AF, U.K.

<sup>3</sup>Laboratoire Nanotechnologies & Nanosystèmes, University of Sherbrooke, Sherbrooke, QC J1K 0A5, Canada

<sup>4</sup>Institute of Electronics, Microelectronics and Nanotechnology, University of Lille, 59650 Lille, France

Corresponding author: Khaled Ahmeda (717828@swansea.ac.uk)

**ABSTRACT** The interplay of self-heating and polarization affecting resistance is studied in AlGa<sub>N</sub>/Ga<sub>N</sub> transmission line model (TLM) heterostructures with a scaled source-to-drain distance. This paper is based on meticulously calibrated TCAD simulations against I–V experimental data using an electro-thermal model. The electro-thermal simulations show hot-spots (with peak temperature in a range of ~566 K–373 K) at the edge of the drain contact due to a large electric field. The electrical stress on Ohmic contacts reduces the total polarization, leading to the inverse/converse piezoelectric effect. This inverse effect decreases the polarization by 7%, 10%, and 17% during a scaling of the source-to-drain distance in the 12 μm, 8 μm, and 4 μm TLM heterostructures, respectively, when compared with the largest 18-μm heterostructure.

**INDEX TERMS** III–V nitrides, self-heating, polarization, TLM structures, electro-thermal transport simulations.

## I. INTRODUCTION

Gallium Nitride (Ga<sub>N</sub>) wide bandgap material possesses attractive properties such as a high breakdown electric field of 3.3 MV/cm, a large carrier mobility in two-dimensional electron gas (2DEG) of 2000 cm<sup>2</sup>/V.s, a large saturation velocity of 2.5 × 10<sup>7</sup> cm/s, a large energy bandgap of 3.4 eV, a low relative permittivity of 10.4, and a high thermal conductivity (κ) of 130 Wm<sup>-1</sup>K<sup>-1</sup> [1], [2]. In addition, III-Nitride based semiconductors possess a large polarization, which is the result of an asymmetrical distribution of electron clouds. Therefore, spontaneous and piezoelectric polarizations play a vital role in AlGa<sub>N</sub>/Ga<sub>N</sub> heterostructure based devices. The polarization together with a large band discontinuity at the AlGa<sub>N</sub>/Ga<sub>N</sub> heterostructure interface lead to a very effective creation of a 2DEG [3]. All these properties offer a range of options to design highly effective power electronics devices using concept of High Electron Mobility Transistors (HEMTs), which are urgently required for variety of future power and high frequency in electronic applications [4]–[6].

In this paper, we study electro-thermal behavior of scaled AlGa<sub>N</sub>/Ga<sub>N</sub> Transmission Line Model (TLM) heterostructures with low resistive Ohmic contacts aimed for AlGa<sub>N</sub>/Ga<sub>N</sub> HEMTs. Understanding the physical transport

process in the contacts is crucial for the following reasons: (1) reducing on-resistance to minimize power loss in Ohmic contacts and (2) achieving a higher extrinsic transconductance ( $g_m$ ) resulting in the increment of current gain and cut-off frequency [7]. The fabrication and specification of AlGa<sub>N</sub>/Ga<sub>N</sub> TLM heterostructures is described in Section II. Sections III and IV outline the simulation methodology and the impact of both self-heating and polarization effects on the device performance. Conclusions are drawn in Section V.

## II. ALGAN/GAN TLM HETEROSTRUCTURE

The studied epi-structure was grown by molecular beam epitaxy (MBE) on HP-Si [111] substrate with a thickness of ~480 μm followed by a 1.7 μm Al<sub>0.1</sub>Ga<sub>0.9</sub>N back-barrier layer, to reduce alloy scattering and to improve the carrier confinement in the 2DEG, followed by a 15 nm Ga<sub>N</sub> channel. A 1 nm AlN spacer was used to reduce alloy disorder scattering and enhance electron mobility in the channel [8], followed by a 25 nm undoped Al<sub>0.32</sub>Ga<sub>0.68</sub>N barrier and a 1 nm Ga<sub>N</sub> cap layer. In an attempt to reduce the contact resistance, the source-to-drain terminal is formed by rapid thermal annealing of an evaporated Ti/Al/Ni/Au (10/200/40/100 nm) multilayer metallisation scheme at 870° C for 30 seconds under nitrogen atmosphere. The devices are electrically isolated by He<sup>+</sup> ion

multiple implantations. To reduce trapping effects and dispersion, the surface of the devices are  $N_2O$  pre-treated for two minutes followed by  $SiO_2/Si_3N_4$  (100/50 nm) bi-layer passivation, performed by plasma-enhanced chemical vapor deposition (CVD) at  $340^\circ C$ . The passivation layer is opened by using a  $CHF_3/CF_4$  reactive ion etching plasma. Before taking any measurements,  $V_{DS} = 0 V$  is applied for a period of time,  $t > 10$  seconds, to fully recover the device from the deleterious phenomena of charge trapping and self-heating that can distort further measurements. The trace of drain current is reproducible showing that no permanent degradation of the drain current occurs in experiment but only recoverable degradation, i.e., due to charge trapping and self-heating. The fabrication process flow is similar to that reported in [9] with  $Si_3N_4$  passivation.

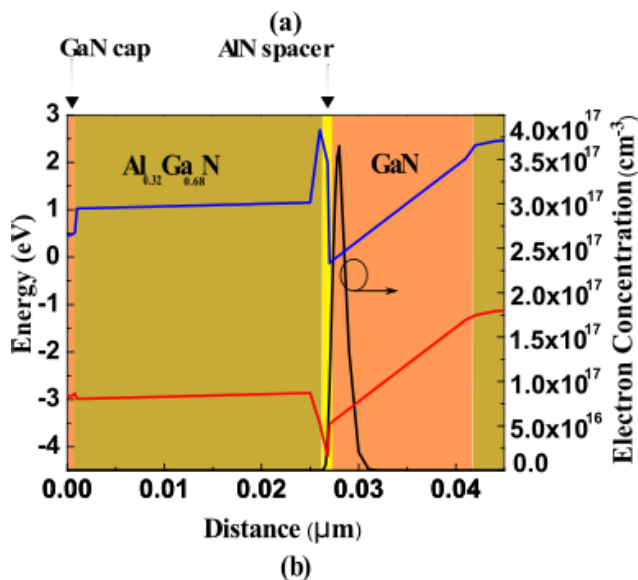
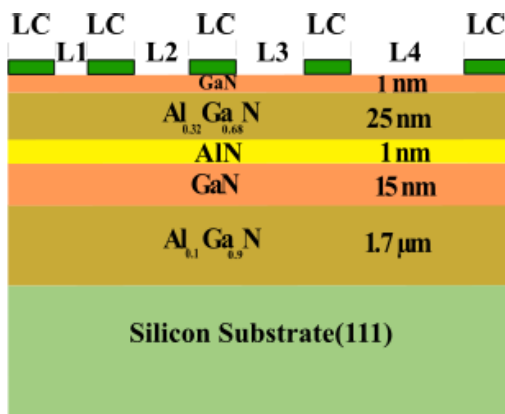


**FIGURE 1.** (a) Schematic cross section of the AlGaN/GaN TLM structure and (b) energy band diagram and electron concentration profile at equilibrium.

The spacing between the Ohmic contacts varies from  $L1 = 4 \mu m$ ,  $L2 = 8 \mu m$ ,  $L3 = 12 \mu m$  and  $L4 = 18 \mu m$ . The Ohmic contact length is  $LC = 50 \mu m$  for all the source-to-drain distances as depicted in Fig. 1(a). The energy band

diagram overlapped with electron concentration profile in the heterostructure cross-section is illustrated in Fig. 1(b). The described Ti/Al/Ni/Au multilayer metallisation scheme was used for Ohmic contacts to create TLM heterostructures with various source-to-drain distances. Hall-effect measurements indicate a 2DEG electron mobility of  $1950 cm^2/V.s$ , at room temperature. A C-V technique has revealed an electron sheet density of  $n_s = 1.5 \times 10^{13} cm^{-2}$ . The Ohmic contacts were implemented to the structures by using heavily doped GaN regions with a measured contact resistance of  $0.3 \Omega.mm$ .

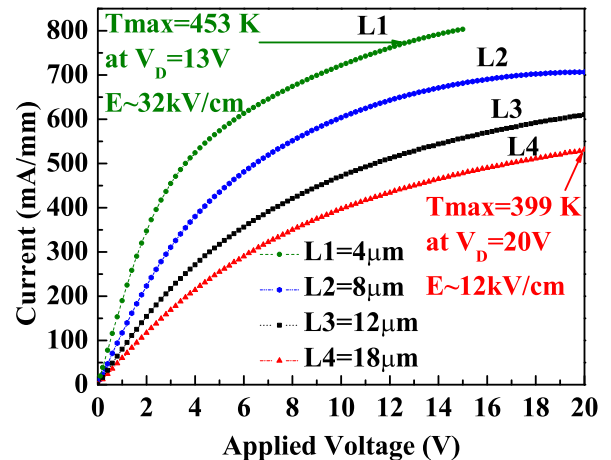


**FIGURE 2.** DC I-V measured characteristics of the AlGaN/GaN TLM structures. The arrows indicate the bias at which temperature of the structure shown at the given electric field is measured at the surface.

The I-V characteristics of the  $100 \mu m$  wide TLM structures with the described source-to-drain distances plotted in Fig. 2 are measured at DC and dark conditions using Agilent B1500A framework. For the shortest distance of  $4 \mu m$ , the voltage applied on the contact is restricted to 15 V to prevent contacts damage, while for other spacing lengths of  $8 \mu m$ ,  $12 \mu m$  and  $18 \mu m$ , the maximum applied voltage is set to 20 V. The arrows point to bias points at which a temperature is measured at the structure ( $18 \mu m$  and  $4 \mu m$  TLM structures only) surface close to the drain.

### III. SIMULATION METHODOLOGY FOR THE TLM STRUCTURE WITH VARIOUS SOURCE TO DRAIN DISTANCES

The electro-thermal model used to simulate electron transport in the TLM heterostructures combines two-dimensional (2D) drift-diffusion (DD) simulations with 2D heat transport model. In the calibration at a low electric field shown in Fig. 4(a), we have used a low-field electron mobility of  $1950 cm^2/V.s$ , a saturation velocity of  $1.9 \times 10^7 cm/s$ , [10] within the concentration dependent mobility model, and a contact resistance of  $0.3 \Omega.mm$ . At a high electric field, a combination of the nitride specific field dependent mobility model [11] with Shockley-Read-Hall (SRH) recombination and Fermi-Dirac statistics is used. The Poisson and current continuity equations are solved self-consistently in all simulations [12].

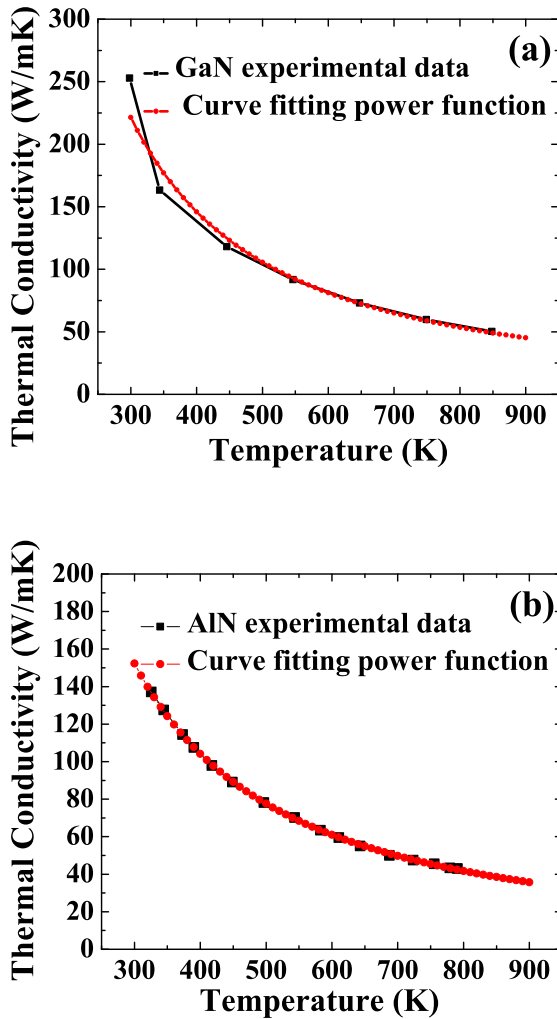


**FIGURE 3.** Thermal conductivity of GaN (a) [21] and AlN (b) [22] as a function of temperature compared with a fitting power function.

Specifically, the low-field analytic mobility model based on Caughey and Thomas [13] and Selberherr [14] is employed in the simulation given by:

$$\mu_n(N, T_L) = \mu_{min} \left( \frac{T_L}{300} \right)^\alpha + \frac{\mu_{max} \left( \frac{T_L}{300} \right)^\beta - \mu_{min} \left( \frac{T_L}{300} \right)^\alpha}{1 + \left( \frac{T_L}{300} \right)^\gamma \left( \frac{N}{N_{crit}} \right)^\delta} \quad (1)$$

where  $N$  and  $T_L$  are the total doping concentration and the temperature in Kelvin,  $\mu_{max}$  and  $\mu_{min}$  are the mobility of undoped samples, where lattice scattering plays a dominant role and the mobility of highly doped materials, where impurity scattering is the main scattering mechanism.  $N_{crit}$  is the doping concentration when the mobility reaches the average value of  $\mu_{max}$  and  $\mu_{min}$ ,  $\delta$  is a measure of how quickly the mobility changes from  $\mu_{max}$  and  $\mu_{min}$ ,  $\delta$ ,  $\beta$  and  $\gamma$  are temperature dependent coefficients.

The AlGaIn/GaN TLM heterostructures have a background doping concentration of  $1 \times 10^{16} \text{ cm}^{-3}$ . Carbon traps density of  $1 \times 10^{17} \text{ cm}^{-3}$  at an energy level  $E_{TC} = E_V + 0.9 \text{ eV}$  and iron traps concentration of  $4 \times 10^{18} \text{ cm}^{-3}$  at

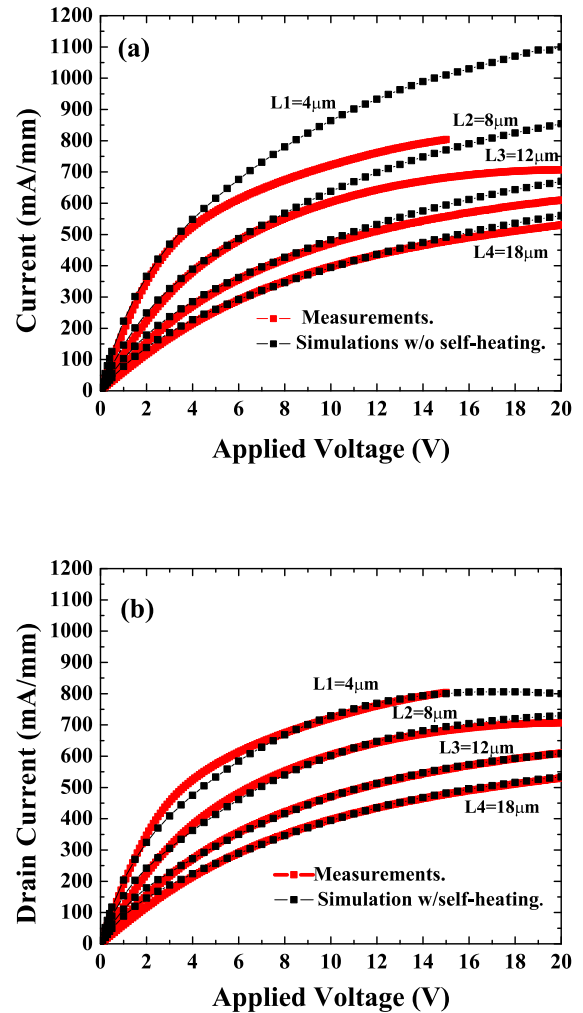


**FIGURE 4.** I-V characteristics of AlGaIn/GaN TLM structure: (a) DD simulations of the AlGaIn/GaN TLM without a self-heating effect, (b) electro-thermal (ET) simulations of the AlGaIn/GaN TLM (with a self-heating effect). Note that the mobility model in the DD and the ET simulations has been calibrated at a low-electric field only.

$E_{TI} = E_V + 0.6 \text{ eV}$  are considered in the GaN buffer and  $Al_{0.1}Ga_{0.9}N$  back barrier, respectively [15]. HP-Si [111] substrate is a  $p$ -type doped [16] with a concentration density of  $5 \times 10^{18} \text{ cm}^{-3}$ . The GaN cap donor concentration was set to be  $5 \times 10^{20} \text{ cm}^{-3}$ , which is similar to that reported in [17] with an energy level of  $E_T = E_C - 0.5 \text{ eV}$  [18]. We simulate a  $8 \mu\text{m}$  thickness of the Si substrate with a bottom thermal contact at  $T = 300 \text{ K}$  but do not introduce additional thermal resistance at the bottom of the simulated structure.

To investigate the impact of self-heating on the device performance, the temperature variations for different source-to-drain distances have been considered. The I-V characteristics of TLM structures are firstly simulated using the DD transport model without considering the self-heating effects to accurately calibrate the low-field mobility and saturation velocity [19] in the linear region of the device, where the self-heating effect is negligible.

Later, self-heating effect is taken into consideration to reproduce the output characteristics as shown in Fig. 4(b).

**TABLE 1.** The fitting coefficients for GaN and AlN used in the relation (2). note that the coefficient  $\alpha_\kappa$  has units of  $W/mK$  while  $\beta_\kappa$  is unitless.

Materials	Coefficient ( $\alpha_\kappa$ ) ( $W/mK$ )	Coefficient ( $\beta_\kappa$ )
GaN	2.2132	1.447
AlN	2.83	1.529

The thermal modelling is activated by Giga module accounting for lattice heat flow in the device [20]. The used values of thermal conductivity of the different layers were taken from [21] and [22]. Giga module in Atlas [12] solves the lattice heat flow equation in addition to the DD and Poisson equations making the overall simulations to be electro-thermal. The heat flow equation is given by:

$$C \frac{\partial T_L}{\partial t} = \nabla(\kappa \nabla T_L) + H \quad (2)$$

where  $C$  denotes the heat capacitance per unit volume,  $\kappa$  is the thermal conductivity of the respective materials,  $H$  is the heat generation term, and  $T_L$  is the local lattice temperature. Thermal conductivity for GaN and AlN has been fit against measured experimental data as presented in Fig. 3. Here, we have used a power function in the form:

$$\kappa(T_L) = \alpha_\kappa \left( \frac{T_L}{300} \right)^{-\beta_\kappa} \quad (3)$$

To fit a dependence of thermal conductivity on temperature with experimental data [21] for GaN and AlN [22] shown in Fig. 3, respectively, that have been used in the simulations.  $\alpha_\kappa$  and  $\beta_\kappa$  are the respective fitting coefficients for GaN and AlN summarized in Table I. The heat generation term is given by the equation [20]:

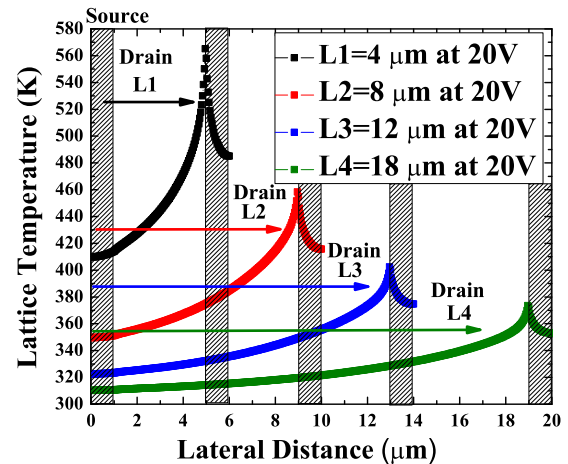
$$H = \left[ \frac{|\vec{j}_n|^2}{q\mu_n n} + \frac{|\vec{j}_p|^2}{q\mu_p p} \right] + q(R - G) \\ [\phi_p - \phi_n + T_L(P_p - P_n)] - T_L(\vec{j}_n \nabla P_n + \vec{j}_p \nabla P_p) \quad (4)$$

where  $\vec{j}_n$ ,  $\vec{j}_p$  are the particle current densities of electrons and holes,  $\mu_n$ ,  $\mu_p$  are the mobility of electrons and holes.  $n$ ,  $p$  are the electron and hole concentrations;  $\phi_n$ ,  $\phi_p$  are the Quasi-Fermi levels of electrons and holes;  $P_p$ ,  $P_n$  are the thermoelectric powers of electrons and holes,  $R$  is the bulk recombination rate of carriers;  $G$  is the carrier generation rate;  $T_L$  is the local lattice temperature; and  $q$  is elementary charge of an electron.

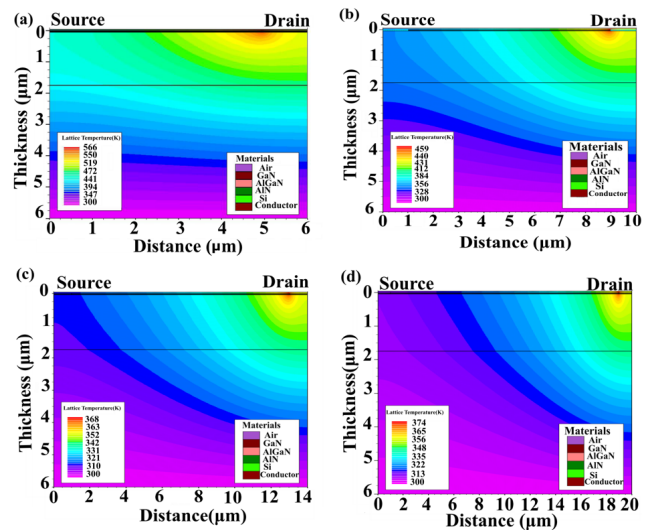
#### IV. THE ROLE OF SELF-HEATING AND POLARIZATION

Fig. 4 shows the calibrated I-V characteristics with and without self-heating effect. Fig. 4(a) presents the calibration of the TLM structure against the experimental measurements without self-heating. A larger difference between the measurement results and the simulations, that is caused by self-heating effect, is seen for the shortest contact spacing of  $L_1 = 4 \mu\text{m}$  at  $V_{DS} = 20 \text{ V}$ . The difference between the

experimental measurements and the simulation data reduces when the source-to-drain distance increases. Fig. 4(b) compares the simulation results obtained from electro-thermal simulations, while using the calibration of thermal conductivity from Fig. 3. A stronger self-heating effect is observed for the shortest source-to-drain distance TLM,  $L_1 = 4 \mu\text{m}$ , when compared with longest TLM,  $L_4 = 18 \mu\text{m}$ . This is due to the higher electric field between the contacts in the shortest TLM compared with larger TLMs. The drain current reduction occurs due to mobility degradation caused by the self-heating. The simulation agreement improves as the distance between the source and drain is increased as expected so a very good agreement between simulation results and measurement data can be observed.



**FIGURE 5.** Lattice temperature profiles in the 2DEG along the channel for different source-to-drain distances at  $V_{DS} = 20 \text{ V}$ .



**FIGURE 6.** 2D Lattice temperature distributions for TLM heterostructures with a source-to-drain distance of  $L_1 = 4 \mu\text{m}$  (a),  $L_2 = 8 \mu\text{m}$  (b),  $L_3 = 12 \mu\text{m}$  (c), and  $L_4 = 18 \mu\text{m}$  (d), at applied biases of 20 V (a, b, c, d), respectively.

The lattice temperature profiles in the 2DEG along the channel and its 2D distributions for all the structures ( $L_1$ ,  $L_2$ ,  $L_3$ , and  $L_4$ ) are presented in Figs. 5 and 6, respectively. When



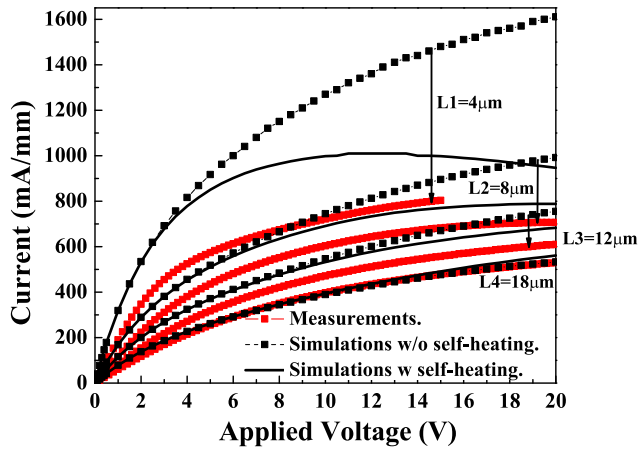


**FIGURE 7.** Measured I-V characteristic of TLM structure (red lines) plotted against the hypothetical low-field calibrated results. The black dashed lines represent the simulations without self-heating while the black solid lines are the simulation results including self-heating effects. In all simulations, the polarization value of the largest structure ( $L4 = 18 \mu\text{m}$ ) is used.

the spacing between the source and the drain decreases, which increases the electric field at the vicinity of the drain [23] in a TLM structure, the lattice temperature increases and hence degrades the transport properties [24]. The GaN channel temperature increase is due to more energetic carriers in the channel with a larger kinetic energy accelerated by the increasing electric field [24]–[26]. The hot spot is located next to the drain contact for all structures [27]. At an applied drain-to-source bias of 20 V, the shortest structure ( $L1 = 4 \mu\text{m}$ ) exhibits a peak lattice temperature of 566 K which is reported similarly in [25]. When the source-to-drain distance increases to  $8 \mu\text{m}$ , a peak of lattice temperature decreases to 459 K in the structure (L2) and then to 403 K and to 374 K in the  $12 \mu\text{m}$  and  $18 \mu\text{m}$  structures (L3 and L4). The hot spot remains at the drain side for all TLM structures [28], [29]. The maximum simulated lattice temperature of 374 K at applied bias of 20 V in the  $18 \mu\text{m}$  TLM structure is in a reasonable agreement ( $\sim 7\%$ ) with a measured temperature of 399 K indicated in Fig. 2. In the smallest,  $4 \mu\text{m}$  TLM structure, the simulations give a lattice temperature of 434 K at applied bias of 13 V (used in the experiment) which is also in a good agreement ( $\sim 4\%$ ) with experimentally measured temperature of 453 K (Fig. 2).

The drain current in the largest TLM structure with a drain-source distance of  $L4 = 18 \mu\text{m}$  is compared against the scaled structures at an applied voltage  $V_{DS} = 15 \text{ V}$  excluding and including the self-heating effects. The self-heating effect has a very small impact on the current of the  $18 \mu\text{m}$  TLM structure. When the distance between the source and drain contacts is reduced to  $L3 = 12 \mu\text{m}$ , the drain current increases by 31.7 % (self-heating included) and by 40.7 % (self-heating excluded). Further scaling of the distance between the source and drain contact to  $L2 = 8 \mu\text{m}$ , the drain current increases by 61.7 % in the simulation with self-heating and 88 % without self-heating. Finally, for the shortest TLM structure of  $L1 = 4 \mu\text{m}$ , the drain

current increases by 109.6 % with self-heating included and by 210.9 % with self-heating excluded in the simulation as compared to the largest TLM structure ( $L4 = 18 \mu\text{m}$ ), which serves here as a reference to the comparison. When applying an external electrical stress on the TLM structure (applied voltage) via contacts, the wurtzite crystal structure of III-Nitrides suffers from the stress. This affects the polarization along with different spacing between the contacts. This phenomenon is known as the inverse or converse piezoelectric effect [29], [30].

To study this phenomenon, we altered the polarization factor for TLM structures to mimic the electrical stress that is applied after each measurement thus changing the total value of polarization. Fig. 7 illustrates hypothetical I-V characteristics if the polarization factor would be fixed at a value calibrated for the TLM structure with  $L4 = 18 \mu\text{m}$ , the largest source-to-drain distance. By applying this value on  $L1 = 4 \mu\text{m}$ , the drain current has increased by 66.8 % in the simulation, which clearly disagrees with experimental observations.

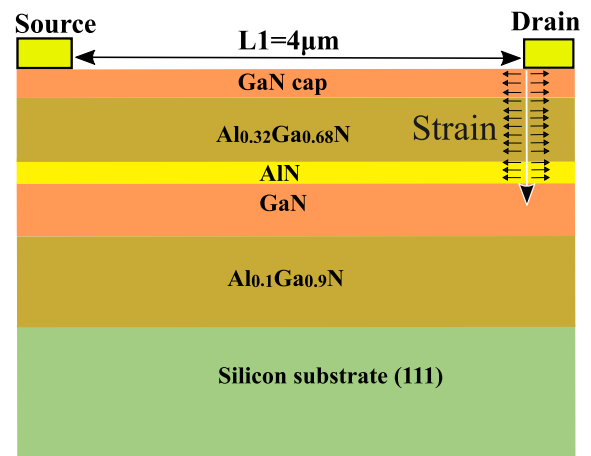


**FIGURE 8.** Schematic diagram of the TLM structure that illustrates the strain induces by applied electrical stress.

Electrical and mechanical strain/stress and its relationship with the electric field in GaN HEMTs has a tremendous impact on GaN based devices in general [29]. Nitride materials like GaN which have unique properties due to the lack of inversion symmetry and high ionicity exhibit inverse/converse piezoelectric effect due to strain/stress generated by the electric field [31]. When applying an external electrical and mechanical stress on the TLM structure via contacts (applied voltage), the wurtzite crystal structure of III-Nitrides suffers distortion and deformation from mechanical stress on GaN and AlGa<sub>N</sub> layers. This affects the polarization along with different spacing between the contacts. The electrical stress caused by an applied voltage on Ohmic contacts induces a lattice deformation at the vicinity of the drain as illustrated in Fig. 8. The total polarization value decreases when compared to the largest contact of  $18 \mu\text{m}$  for  $12 \mu\text{m}$ ,  $8 \mu\text{m}$ , and  $4 \mu\text{m}$  by 7 %, 10 %, and 17 %, respectively.

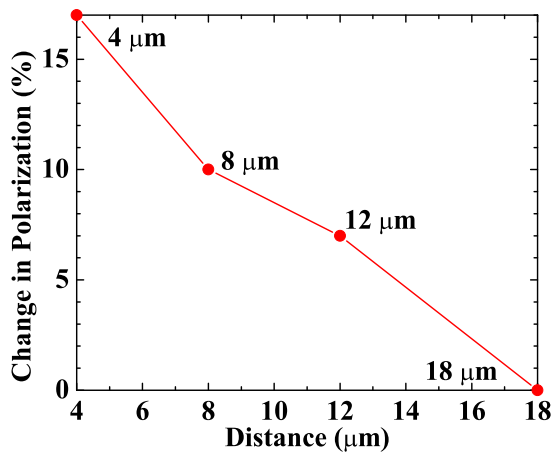


**FIGURE 9.** The total polarization value decreases when compared to the total polarization used in the largest 18 μm TLM structure.

The relationship between the change-in-polarization and the source-to-drain distance is almost linear, as shown in Fig 9.

## V. CONCLUSIONS

We have studied  $\text{Al}_{0.32}\text{Ga}_{0.68}\text{N}/\text{AlN}/\text{GaN}/\text{Al}_{0.1}\text{Ga}_{0.9}\text{N}$  TLM heterostructures with a GaN cap layer grown on a *p*-type doped HP-Si [111] substrate. Their I-V characteristics from experimental measurements were simulated via a 2D drift-diffusion transport model using Fermi-Dirac statistics and the SRH recombination model by commercial tool Atlas-Silvaco [12]. Thermal model was employed to study the self-heating effects with the thermal conductivity approximated by a power function and calibrated to experimental data. We have found that the current soon becomes limited by increase in a lattice temperature with the increase in applied bias up to 13% (the 4 μm structure) and that this limitation occurs sooner in shorter structures. We have demonstrated a good agreement of the electro-thermal simulations predicting a lattice temperature of 374 K against experimental temperature of 399 K at applied bias of 20 V in the largest, 18 μm structure as well as in the smallest, 4 μm structure, predicting a lattice temperature of 434 K against experimental temperature of 453 K at applied bias of 13 V. The maximum lattice temperature (for instance ~ 566K in the 4 μm structure at  $V_{DS} = 20$  V) was predicted in the vicinity of the drain. In addition, we have observed that, by applying electrical stress (voltage) on the Ohmic contacts, the total polarization value in heterostructure reduces when compared to the largest contact distance of 18 μm for 12 μm, 8 μm, and 4 μm by 7 %, 10 %, and 17%, respectively. This decrease in the total polarization is due to the inverse piezoelectric effect, or also called the converse piezoelectric effect, caused by the additional stress induced by the applied electric field on contact. The inverse piezoelectric effect changes the total polarization thus affecting a 2DEG density in the channel [29], [30], [32].

## REFERENCES

- [1] M. Ishida, Y. Uemoto, T. Ueda, T. Tanaka, and D. Ueda, "GaN power switching devices," in *Proc. Int. Power Eng. Conf. (IPEC)*, Jun. 2010, pp. 1014–1017.
- [2] R. J. Trew, "High-frequency solid-state electronic devices," *IEEE Trans. Electron Devices*, vol. 52, no. 5, pp. 638–649, May 2005.
- [3] R. Vetury, N. Q. Zhang, S. Keller, and U. K. Mishra, "The impact of surface states on the DC and RF characteristics of AlGaIn/GaN HFETs," *IEEE Trans. Electron Devices*, vol. 48, no. 3, pp. 560–566, Mar. 2001.
- [4] E. A. Jones, F. F. Wang, and D. Costinett, "Review of commercial GaN power devices and GaN-based converter design challenges," *IEEE J. Emerg. Sel. Topics Power Electron.*, vol. 4, no. 3, pp. 707–719, Sep. 2016.
- [5] S. L. Delage and C. Dua, "Wide band gap semiconductor reliability: Status and trends," *Microelectron. Rel.*, vol. 43, nos. 9–11, pp. 1705–1712, Sep. 2003.
- [6] H.-Q. Tao, W. Hong, B. Zhang, and X.-M. Yu, "A compact 60W X-band GaN HEMT power amplifier MMIC," *IEEE Microw. Wireless Compon. Lett.*, vol. 27, no. 1, pp. 73–75, Jan. 2017.
- [7] S. Taking, "AlN/GaN MOS-HEMTs technology," Ph.D. dissertation, Division Electron. Nanoscale Eng., School Eng., Univ. Glasgow, Glasgow, Scotland, 2012.
- [8] I. P. Smorchkova et al., "AlN/GaN and (Al,Ga)N/AlN/GaN two-dimensional electron gas structures grown by plasma-assisted molecular-beam epitaxy," *J. Appl. Phys.*, vol. 90, no. 10, p. 5196, Nov. 2001.
- [9] A. Soltani et al., "Power performance of AlGaIn/GaN high-electron-mobility transistors on (110) silicon substrate at 40 GHz," *IEEE Electron Device Lett.*, vol. 34, no. 4, pp. 490–492, Apr. 2013.
- [10] S. Bajaj et al., "Density-dependent electron transport and precise modeling of GaN high electron mobility transistors," *Appl. Phys. Lett.*, vol. 107, no. 15, p. 153504, Oct. 2015.
- [11] M. Farahmand et al., "Monte Carlo simulation of electron transport in the III-nitride wurtzite phase materials system: Binaries and ternaries," *IEEE Trans. Electron Devices*, vol. 48, no. 3, pp. 535–542, Mar. 2001.
- [12] *Atlas Users Manual, Device Simulation Software*, Silvaco Int., Santa Clara, CA, USA, 2016.
- [13] R. E. Thomas, "Carrier mobilities in silicon empirically related to doping and field," *Proc. IEEE*, vol. 55, no. 12, pp. 2192–2193, Dec. 1967.
- [14] S. Selberherr, "Process and device modeling for VLSI," *Microelectron. Rel.*, vol. 24, no. 2, pp. 225–257, 1984.
- [15] M. J. Uren, J. Moreke, and M. Kuball, "Buffer design to minimize current collapse in GaN/AlGaIn HFETs," *IEEE Trans. Electron Devices*, vol. 59, no. 12, pp. 3327–3333, Dec. 2012.
- [16] E. M. Chumbes et al., "AlGaIn/GaN high electron mobility transistors on Si(111) substrates," *IEEE Trans. Electron Devices*, vol. 48, no. 3, pp. 420–426, Mar. 2001.
- [17] J. Kuzmik et al., "Proposal and performance analysis of normally off  $n^{++}$  GaN/InAlN/AlN/GaN HEMTs with 1-nm-thick InAlN barrier," *IEEE Trans. Electron Devices*, vol. 57, no. 9, pp. 2144–2154, Sep. 2010.
- [18] Y.-J. Lin, Q. Ker, C.-Y. Ho, H.-C. Chang, and F.-T. Chien, "Nitrogen-vacancy-related defects and Fermi level pinning in *n*-GaN Schottky diodes," *J. Appl. Phys.*, vol. 94, no. 3, pp. 1819–1822, Aug. 2003.
- [19] B. E. Foutz, S. K. O'Leary, M. S. Shur, and L. F. Eastman, "Transient electron transport in wurtzite GaN, InN, and AlN," *J. Appl. Phys.*, vol. 85, no. 11, pp. 7727–7734, Jun. 1999.
- [20] G. K. Wachutka, "Rigorous thermodynamic treatment of heat generation and conduction in semiconductor device modeling," *IEEE Trans. Comput.-Aided Des. Integr. Circuits Syst.*, vol. 9, no. 11, pp. 1141–1149, Nov. 1990.
- [21] V. Palankovski and R. Quay, *Analysis and Simulation of Heterostructure Devices*. Vienna, Austria: Springer-Verlag, 2004, pp. 44–45.
- [22] H. Shibata et al., "High thermal conductivity of gallium nitride (GaN) crystals grown by HVPE process," *Mater. Trans.*, vol. 48, no. 10, pp. 2782–2786, Sep. 2007.
- [23] S. Rajasingam et al., "Micro-Raman temperature measurements for electric field assessment in active AlGaIn-GaN HFETs," *IEEE Electron Device Lett.*, vol. 25, no. 7, pp. 456–458, Jul. 2014.
- [24] B. Benbakhti, A. Soltani, K. Kalna, M. Rousseau, and J.-C. De Jaeger, "Effects of self-heating on performance degradation in AlGaIn/GaN-based devices," *IEEE Trans. Electron Devices*, vol. 56, no. 10, pp. 2178–2185, Oct. 2009.
- [25] W. H. Tham et al., "Comparison of the Al<sub>1-x</sub>Ga<sub>x</sub>N/GaN heterostructures grown on silicon-on-insulator and bulk-silicon substrates," *IEEE Trans. Electron Devices*, vol. 63, no. 1, pp. 345–352, Jan. 2016.
- [26] M. Faqir, G. Verzellesi, G. Meneghesso, E. Zanoni, and F. Fantini, "Investigation of high-electric-field degradation effects in AlGaIn/GaN HEMTs," *IEEE Trans. Electron Devices*, vol. 55, no. 7, pp. 1592–1602, Jul. 2008.

- [27] T. Sadi, R. W. Kelsall, and N. J. Pilgrim, "Investigation of self-heating effects in submicrometer GaN/AlGaN HEMTs using an electrothermal Monte Carlo method," *IEEE Trans. Electron Devices*, vol. 53, no. 12, pp. 2892–2900, Dec. 2006.
- [28] J. Kuzmík et al., "Self-heating in GaN transistors designed for high-power operation," *IEEE Trans. Electron Devices*, vol. 61, no. 10, pp. 3429–3434, Oct. 2014.
- [29] U. Chowdhury et al., "TEM observation of crack- and pit-shaped defects in electrically degraded GaN HEMTs," *IEEE Electron Device Lett.*, vol. 29, no. 10, pp. 1098–1100, Oct. 2008.
- [30] R. Chu, "Gate-recessed GaN high electron mobility transistors with scaled gate length," Ph.D. dissertation, Dept. Elect. Electron. Eng., Univ. California, Santa Barbara, Santa Barbara, CA, USA, Dec. 2008.
- [31] D. Sztenkiel et al., "Stretching Magnetism with an Electric Field in a Nitride Semiconductor," *Nature Commun.*, vol. 7, Oct. 2016, Art. no. 13232.
- [32] J. Joh, L. Xia, and J. A. del Alamo, "Gate current degradation mechanisms of GaN high electron mobility transistors," in *IEDM Tech. Dig.*, Dec. 2007, pp. 385–388.



**KHALED AHMEDA** received the B.Eng. degree of electrical and electronics engineering from the College of Petroleum Engineering, Al-Briga, Sirte University, Libya, in 2003, and the M.Sc. degree in microelectronics from Universiti Kebangsaan Malaysia, Bangi, Malaysia, in 2005. In 2006, he became an Assistant Lecturer with Sirte University. He is currently pursuing the Ph.D. degree with Swansea University, where he is involved on the research on reliability of GaN HEMTs for power and RF applications.



**BRENDAN UBOCHI** received the B.Eng. and M.Sc. degrees from the Federal University of Technology, Owerri, Nigeria, and The University of Manchester, U.K., in 2007 and 2011, respectively. He is currently pursuing the Ph.D. degree with Swansea University, U.K. He joined the Federal University of Technology, Akure, Nigeria, in 2012. His current research interests include device physics and modeling of semiconductor devices for power and radio frequency applications.



**BRAHIM BENBAKHTI** received the M.Sc. and Ph.D. degrees in microwave and microtechnology from Lille University, Lille, France, in 2003 and 2007, respectively. He is currently with the Electronics and Electrical Engineering Department, Liverpool JMU, Liverpool, U.K. His current research interests include reliability characterization and simulation of III-nitrides-based devices, transistor structure engineering, nanoscale III-V, and Ge channel MOSFETs.



**STEVEN J. DUFFY** received the B.Eng. degree in electrical and electronics engineering and the M.Sc. degree in microelectronic systems design from Liverpool John Moores University (LJMU), Liverpool, U.K., in 2014 and 2015, respectively. During his M.Sc. project, he developed his interest in the reliability and thermal analysis of GaN-based devices. He is currently pursuing the Ph.D. degree in reliability characterization of III-Nitrides-based devices for technology development with LJMU.



**ALI SOLTANI** received the B.Sc. degree in theoretical physics and the M.Sc. degree in optoelectronic from Lorraine University, Nancy, France, in 1994 and 1996, respectively, and the Ph.D. degrees in electrical engineering from Metz University, and Supelec, Gif-sur-Yvette, France, in 2001. His current research interests include the Al(Ga)N/GaN resonant tunneling diodes, X-UV photodetectors, elastic wave sensors, the design and fabrication of wide bandgap, high-power, and high-frequency devices.



**WEI DONG ZHANG** received the Ph.D. degree from Liverpool John Moores University (LJMU), Liverpool, U.K., in 2003. He is currently a Professor of nanoelectronics with LJMU. His research interests include the characterization and quality assessment of nanoscale resistive switching and flash memory devices, CMOS devices, and GaN HEMT devices.



**KAROL KALNA** received the M.Sc. degree (Hons.) in solid state physics and the Ph.D. degree in condensed matter physics from Comenius University, Bratislava, Czechoslovakia, in 1990 and 1998, respectively. He has been currently an Associated Professor with Swansea University, Wales, U.K., since 2012, and a Co-Leader of Nanoelectronic Devices Computational Group and a Leader of GaN Devices Modeling Group. In 1994, he joined the Institute of Electrical Engineering,

Slovak Academy of Sciences, Bratislava, Slovakia, as a Research Scientist. He was a Visiting Post-Graduate Student with the Department of Physics, UIA University of Antwerp, Belgium, where he involving on semiconductor lasers modeling, in 1994 and 1997. From 1999 to 2010, he was with the Department of Electronics and Electrical Engineering, University of Glasgow, Scotland, U.K., where he was studying the scaling of high electron mobility transistor (HEMT) into sub-100 nm dimensions performing DC and RF analysis within ensemble Monte Carlo simulations. From 2002, he pioneered III-V MOSFETs for future digital technology studying transistor scaling with Monte Carlo simulations. From 2007 to 2012, he was an Engineering and Physical Sciences Research Council Advanced Research Fellow carrying out the Monte Carlo modeling of deep sub-100 nm, ultra-thin body transistors with Si and high mobility materials in a channel. In 2010, he became a Senior Lecturer with the College of Engineering, Swansea University, Wales, U.K., establishing his own Nanoelectronic Devices Computational Group. He has over 200 publications, including 82 papers in peer-review journals and 20 invited talks. His research interests include finite element 2-D and 3-D Monte Carlo simulations of nanoscaled MOSFETs, including FinFETs and nanowires with a channel based on Si, strain Si, and III-V semiconductors; quantum transport simulations using non-equilibrium Green's functions; multiscale modeling of nanoscale contacts; simulations of ZnO nanowires, and simulations of GaN-based HEMTs. He has served in program committee of 2009, 2011 IEEE Nano, ULIS 2010, and EDISON 2015 conferences. He was the Chair of Program Committee of IWCN 2017.

...